EFFICIENT AND RELIABLE SURGE PREVENTION ALGORITHM FOR CENTRIFUGAL COMPRESSOR

Grzegorz Liskiewicz

Lodz University of Technology, Institute of Turbomachinery

POLAND

ABSTRACT

The paper presents an outline of a technology of the active anti-surge algorithm based on high-frequency pressure measurement. The presented system is very fast, inexpensive, reliable and does not limit the machine operating range. Many contemporary anti-surge systems are based on theoretical surge margin. This solution limits machine operating range by about 10-15 percent in the region of the highest pressure ratios. It is also often sensitive to change of external conditions such as temperature or density as the system reacts to limits calculated theoretically. The presented safety system uses the signal to develop the so-called RDF parameter. In nominal working conditions, this parameter keeps the value close to 1. When RDF reaches values over 3 the anti-surge procedure should be implemented. Experimental studies have shown that this algorithm assures enough time to incur actions suppressing unstable phenomena. The system reacts to real machine working conditions and is, hence, reliable. The RDF algorithm could be also used to identify local flow instabilities as well as off-design operation. We are looking for a development partner willing to test and implement this solution on their machines. All described experiments were conducted for the case of centrifugal impellers, however, we are open to making tests on axial machines.

1 INTRODUCTION

1.1 Classification of Unstable Flow Structures

Whenever a compressing machine operates at a given rotational speed and the flow is continuously reduced, there is usually a moment after which the stage will no longer operate in a stable manner. Therefore, it is very important to accurately predict the point at which instabilities are likely to occur. However, there are many larger and smaller disturbances that are influencing the flow stability. The most common words used in reference to unstable working conditions are the **surge** and the **stall**. Although they are different phenomena, these words are commonly used, or misused, to describe the same phenomenon or unstable operating conditions in general. This section is intended to provide brief classification of the unstable flow phenomena which was used in this study. It was based on definitions given in different textbooks including Frigne and van den Braembussche [1], Izmaylov [2], Greitzer [3].

Each unstable flow structure is associated with oscillations of flow parameters which are propagating in a certain direction. Instability can be global, i.e. influence the machine with the inlet and the outlet sections or appear lo-

cally in one machine section. Each part of the compressing machine is characterized by different flow structures with different instability onset mechanisms.

- **Surge** - global flow fluctuations in the axial direction.

- **Rotating Stall** - local circumferential flow fluctuations. Depending on the place of occurrence it can be classified as [4]

  - **Progressive Impeller Rotating Stall** - appearing in the inducer zone. This structure is usually connected with gradual drop of the machine pressure ratio, hence the name "progressive".

  - **Abrupt Impeller Rotating Stall** - appearing close to the impeller outlet. This structure is usually connected with sudden drop of the machine pressure ratio, hence the name "abrupt".

  - **Vaneless Diffuser Rotating Stall** - appearing in the diffuser.

- **Inlet Recirculation** (IR, also known as the inducer recirculation or inducer backflow) - local flow structure upstream of the impeller. This phenomenon has a form of toroidal flow structure that can be present around the whole circumference.

1.2   Surge

According to [5], the surge phenomenon can be divided into four stages:

- Mild Surge - minor oscillations of the pressure, a reverse flow is not observed.

- Classic Surge - non-linear oscillations, a reverse flow is not observed.

- Modified Surge - classic surge together with the rotating stall.

- Deep Surge - pressure oscillations are large enough to reverse the flow direction periodically.

In fact, it is usually difficult to distinguish between these types and it is common to simply divide them into the mild and the deep surge only [6]. The deep surge corresponds to situation, when oscillations reach the scale leading to global inversion of a flow direction during some part of the cycle. Surge phenomenon was first recognized in the 1950s and has been a subject of extensive research thereafter. The first non-stable phenomena in centrifugal units were identified and analysed by Emmons et al. [7]. In 1976 Greitzer developed a mathematical model of surge onset [8] and confirmed it by experiment [9]. This model, in spite of being originally developed for axial compressing units, was proven to work well in case of the centrifugal machine [10–12].

1.3   Surge Protection

Classic stall protection schemes rely on the detection of typical disturbances preceding its inception [13]. The process of stall initiation is very short and has a timescale comparable to the period of the impeller revolution

[14]. If the pressure instability continues to propagate in the axial direction it may lead to immediate surge inception [15] which appears in the time range roughly one order of magnitude longer than the period of the stall [16]. Then, due to the stated difference in periods, stall and moments of on design compressor operation may spontaneously appear and disappear during a single cycle of the surge [17, 18]. Once started surge may be stoped by adjustment of throttles or bleeds. However, due to hysteresis, the rotating stall may not diminish that easily and it may require the unit to be shut down and restarted [8].

Examination of pressure signals in the frequency domain introduced new insight into the description of rotating stall and surge. As expected, comparison of frequency spectra at the design point to those attained at surge revealed the presence of new harmonic components [19]. The number of local maxima in the spectra reflect the complexity of the non-stable flow structures. It is also possible to observe how the structures propagate throughout the unit by analysing frequency spectra at different working conditions in different locations. In this way Tamaki concluded that the stall inception takes place in the vicinity of a compressor leading edge [15]. Horodko in his work used the continuous wavelet transform (CWT) to obtain time-dependent frequency spectra at the surge onset [18, 20, 21]. Study confirmed that the rotating stall initiates from the vicinity of the impeller leading edge. Similar phenomena were observed in other experiments conducted on different compressing units [22]. However, no complete description of possible flow structures in that region has yet been provided. Vortex structures appear at the leading edge of impeller blades. As the mass flow rate continues to decrease, vortices grow and create a torus-like vortex structure over the whole circumference. This induces a change in the angle of attack of the impeller leading edge and stall is likely to occur.

2 METHOD

A single stage centrifugal blower DP1.12 was the object of investigation. Figure 1 presents the cross-section of the blower and its main dimensions.

The flow enters the rig through the inlet pipe (A) of diameter $D_{in} = 300$ mm. Then, it was accelerated in the Witoszynski nozzle [23] (B) and directed towards the impeller (C). The rotor inlet diameter at the hub equalled $D_{1hub} = 86.3$ mm and the inlet span $b_1 = 38.9$ mm. At the outlet, the diameter and the span equalled $D_2 = 330.0$ mm and $b_2 = 14.5$ mm respectively. The gap between the blade tip and the shroud maintained constant value $\delta = 0.8$ mm along the whole blade. The length of a single impeller passage varied from 174 mm at hub to 134 mm at the shroud giving an average $L_p = 154$ mm. The area of the passage cross-section at the impeller inlet was $A_{p-in} = 823$ mm^2 and $A_{p-out} = 676$ mm^2 at the outlet. Downstream of the rotor, air entered the vaneless diffuser (D). The diffuser outlet diameter was equal to $D_3 = 476$ mm. Afterwards, flow entered the circular volute (E) of radius R_θ. The radius was gradually increasing streamwise from the volute tongue gap of 5 mm towards the outlet pipe of diameter $D_{out} = 150$ mm. The outlet pipe contained two straight sections connected with the right-angle elbow. The section joining the volute and the elbow was 250 mm long, section behind the elbow was 3750 mm long. A throttling valve was mounted at the end of the outlet pipe.

The rotor was driven by an asynchronous AC motor ($400V/15kVA$). The blower was designed to operate at ambient inlet conditions. The unit was run at the rotational speed of $f_{rot} = 100$ Hz with nominal flow rate of $\dot{m}_n = 0.75 \frac{\text{kg}}{\text{s}}$ and pressure ratio $PR = 1.08$. Rotational speed yielded the impeller tip speed equal to $u_{tip} = 103 \frac{\text{m}}{\text{s}}$. The impeller had $z = 23$ blades.

The test stand was equipped with 7 dynamic subminiature Kulite transducers connected to an Iotech Wavebook 516/E data acquisition system. Five of the transducers were mounted flush to the shroud walls to measure the
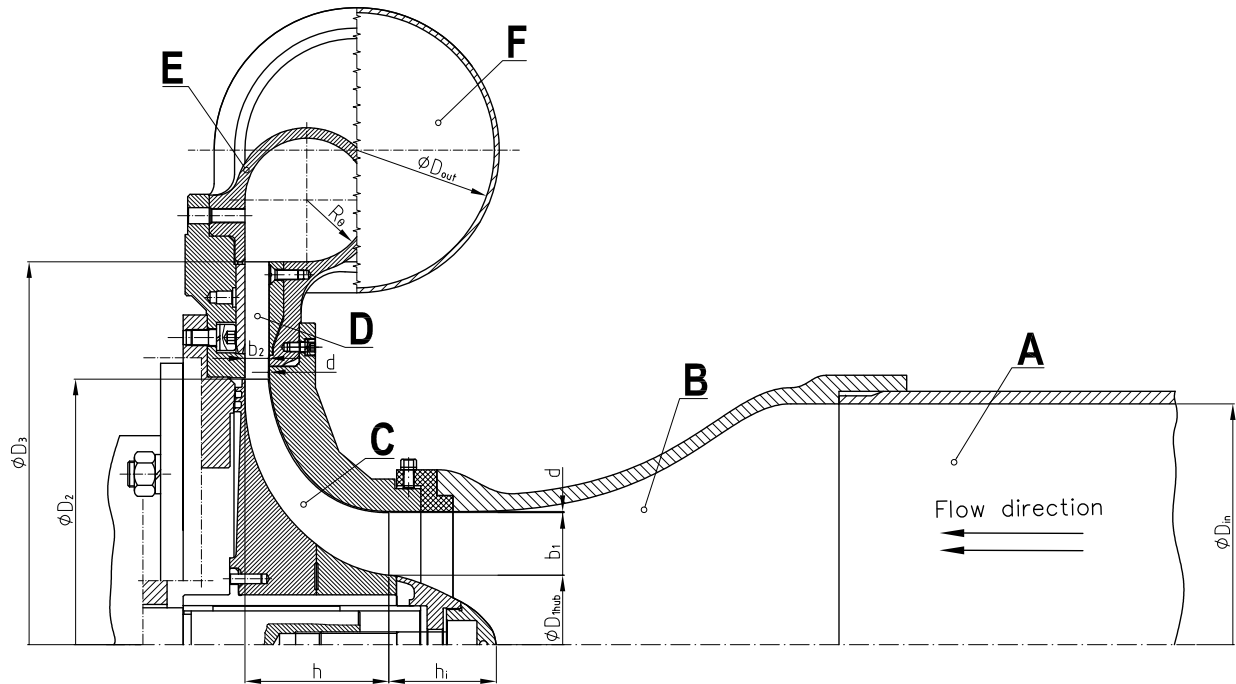
Figure 1: Cross-section of the DP1.12 blower in configuration used in this study with the most important dimensions

static pressure, two were built into Pitot tubes located in the inlet pipe. Gauge positions are presented in figure 2. The list below contains the notation and position of each gauge:

- p_{s-in} - static pressure at the inlet pipe upstream of the Witoszynski nozzle;

- p_{s-out} - outlet static pressure at the volute outlet;

- p_{s-imp1} - static pressures at the impeller shroud, in the inlet zone ($L = -0.2$);

- p_{s-imp2} - static pressures at the impeller shroud, at the mid-chord ($L = 0.4$);

- p_{s-imp3} - static pressures at the impeller shroud, near the trailing edge ($L = 0.9$);

- p_{t-in1}, p_{t-in1} - total pressure at the inlet pipe upstream of the Witoszynski nozzle;

- p_{t-in2} - total pressure at the inlet pipe upstream of the Witoszynski nozzle.

Longitudinal position of the static tappings at the impeller shroud was described by the L dimensionless parameter. It was set to be equal to $L = 0$ at the rotor leading edge and $L = 1$ at the rotor trailing edge.
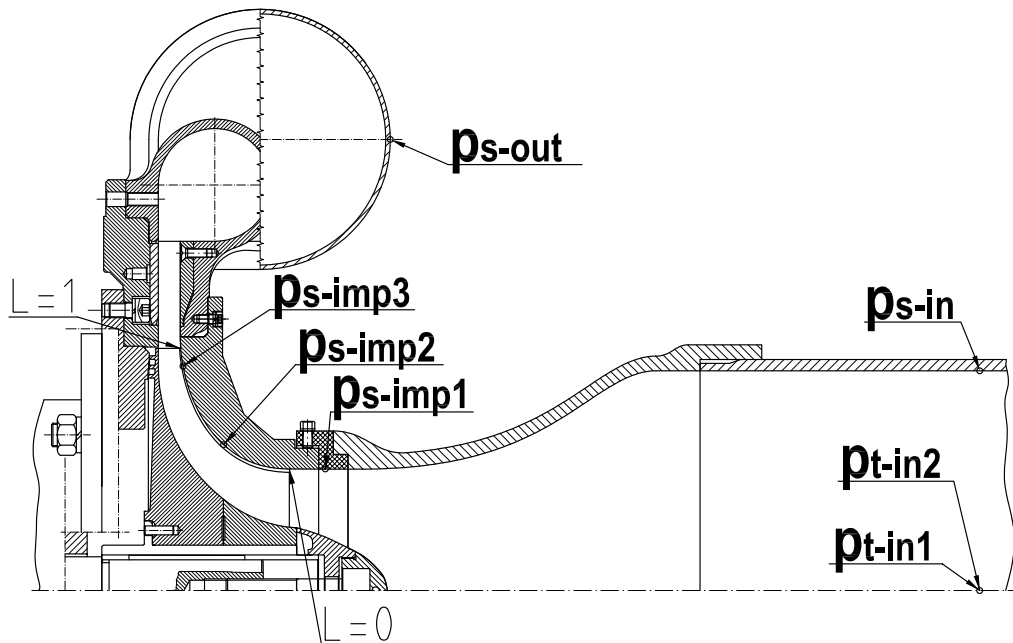
Figure 2: Cross-section of the DP1.12 blower in the configuration used in this study with positions of the pressure gauges

Table 1: Working regimes identified during dynamical tests

Time range	Stability	Gauges	Name
$t < 6$ s	stable	all	nominal work
$t \in (6$ s$, 9$ s$)$	transient	p_{s-imp1}	inlet recirculation
$t \in (9$ s$, 14$ s$)$	unstable	all	transient phase
$t > 14$ s	unstable	all	deep surge

3 RESULTS

3.1 Representation of Signals in the Phase Space

Figures 3-7 present the pressure signals in 3 dimensional phase spaces and their three projections on all two dimensional subspaces. For the sake of clarity the 3-dimensional representations contained only the points registered at the deep surge. All 2-dimensional projections contained the signal registered during the full test, but each phase distinguished in table 1 was marked in different colour.
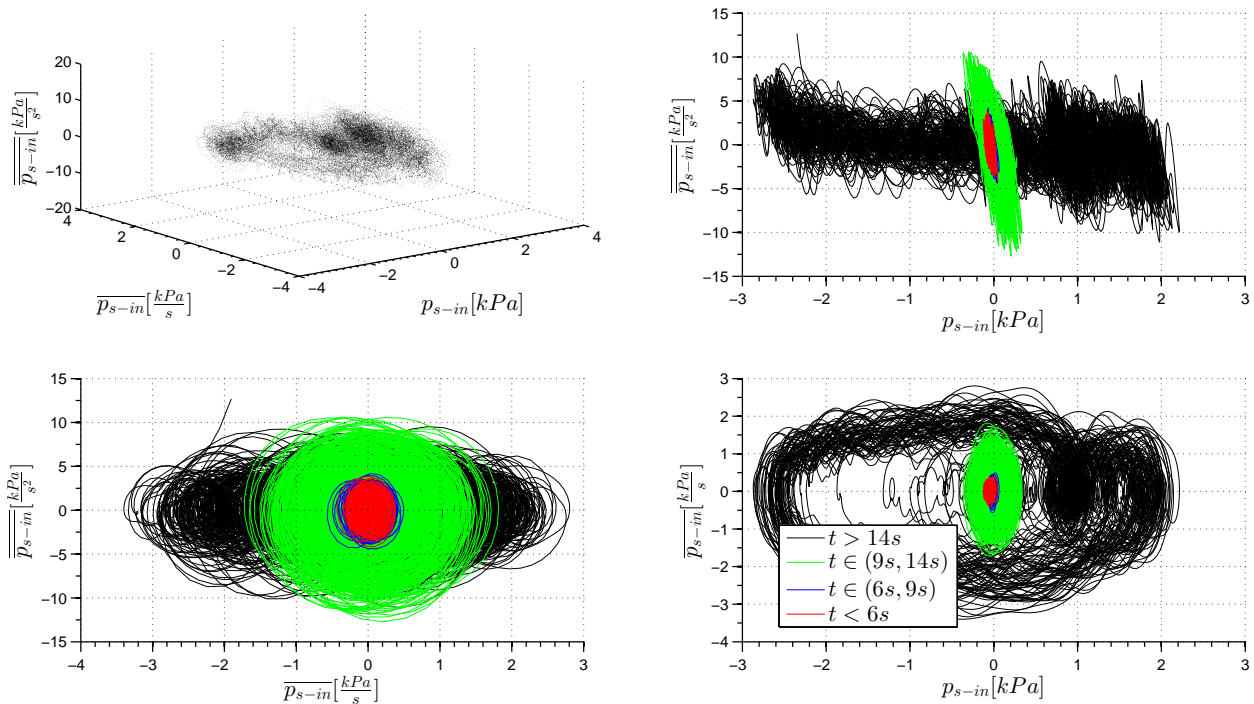

Figure 3: Phase trajectory of the pressure signals registered by gauge p_{s-in} and its projections

Figure 3 presents the phase trajectory of the pressure signal gathered at the inlet. At stable working conditions the signal oscillated in narrow range around $(0, 0, 0)$. It had the form of flat elliptical disc. Higher values of the second derivative were a constant tendency and were caused by the rising influence of noise with the order of derivation. Nevertheless, the scale of oscillations was limited and the phase attractor at $t < 6$ s had undoubtedly a form of a point which meant that the system was dynamically stable. At $t \in (6$ s$, 9$ s$)$ the fluctuations of derivatives were only slightly higher. The system appeared to remain dynamically stable from the point of view of phase portrait of the signal p_{s-in}.

At $t \in (9$ s$, 14$ s$)$ the scale of oscillations increased. Growth of p_{s-in} was observed. However, the relative growth of both derivatives was much higher and the derivatives were noticeably fluctuating around zero which can be observed in projection $\overline{\overline{p_{s-in}}} - \overline{p_{s-in}}$. This observation allowed us to formulate a new parameter indicating appearance of the unstable phenomena. Section 3.2 is devoted to this matter. At deep surge the situation changed dramatically. The projection $\overline{\overline{p_{s-in}}} - \overline{p_{s-in}}$ showed that the range of fluctuation of the first derivative

increased, while the second maintained at the same level of fluctuation. The phase trajectory reached the limit cycle which was much more complicated than a simple ellipse. This reflected a non-linear character of the oscillations. Projection $\overline{p_{s-in}} - p_{s-in}$ exhibited that the origin was very loosely occupied by the points. Therefore, the trajectory was encircling the point of stable operation.

Briefly speaking, the process of entering surge can be described as gradual loss of stability reflected incrementally in fluctuation of both derivatives. At the surge onset, bifurcation appeared from stable attractor located at the point $(0, 0, 0)$ to the limit cycle corresponding to the deep surge. After bifurcation, the pressure started to oscillate noticeably.
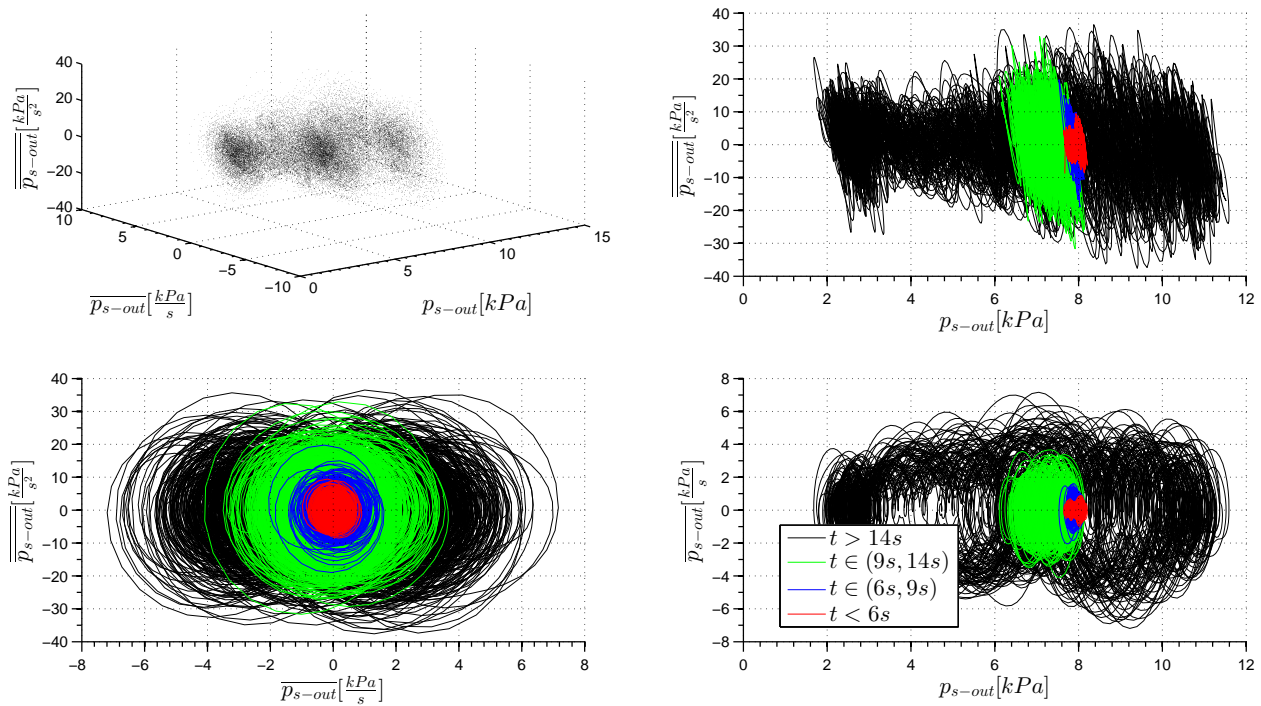

Figure 4: Phase trajectory of the pressure signals registered by gauge p_{s-out} and its projections

Phase trajectory of the outlet pressure signal p_{s-out} presented in figure 4 exhibited some similarities to the previous one. In the stable regime slight oscillations around the stationary point were observed. One can observe that the phase portrait at $t < 6$ s was characterized by small fluctuations of both derivatives. Pressure change was caused by change in the blower pressure head and it could be expected that for fixed working conditions the phase portrait had a shape of an ellipsoid. At $t \in (6\,\mathrm{s}, 9\,\mathrm{s})$ the derivatives fluctuations became slightly higher and at the transient phase they increased again. At the deep surge, the range of fluctuation of the first derivative became higher, while the second derivative maintained at the same level of fluctuation. The pressure p_{s-out} oscillated between 2 kPa and 11 kPa and the limit cycle was observed.

Figure 5 shows the phase trajectory of the pressure signal registered at the shroud in close vicinity of the impeller leading edge. At $t < 6$ s the phase portrait had the form of an ellipsoid which was moving along the p_{s-imp1} axis. One can observe that at the nominal point the pressure was negative due to suction zone formed upstream of the compressor. Afterwards the suction effect diminished and the system entered the inlet recirculation $t \in (6\,\mathrm{s}, 9\,\mathrm{s})$ where the rate of derivative fluctuation increased. The projection $\overline{p_{s-imp1}} - \overline{p_{s-imp1}}$ clearly
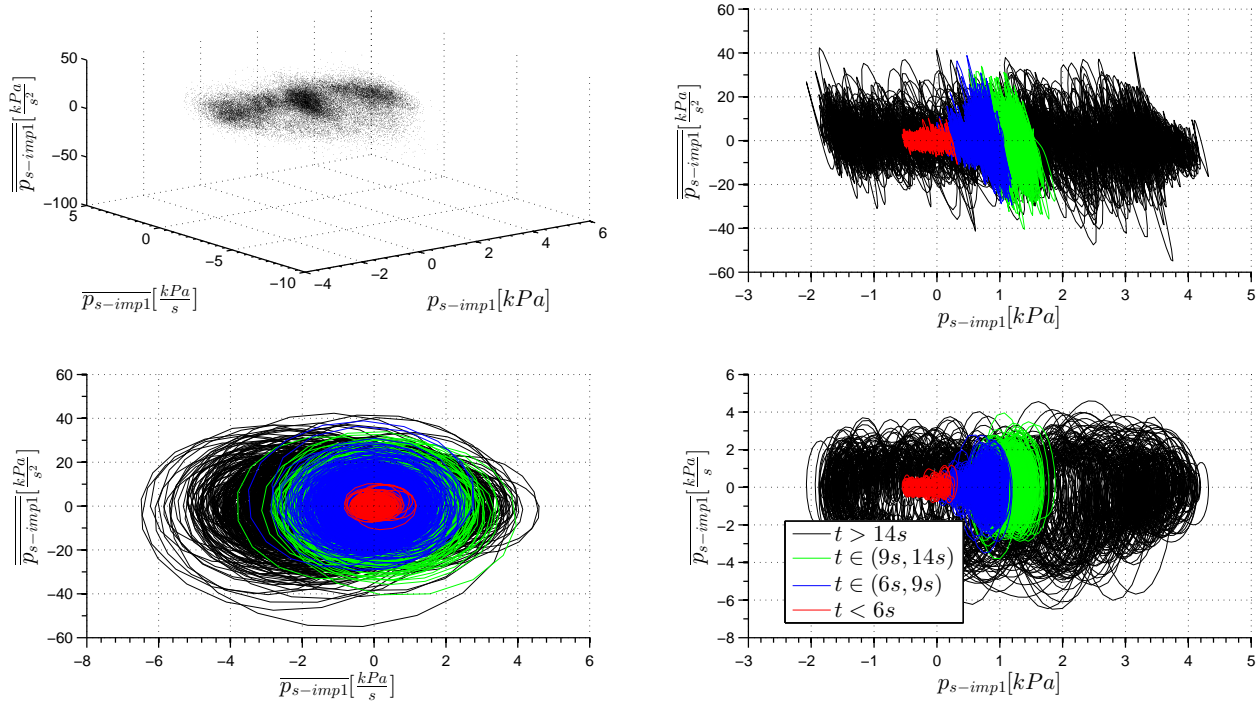
Figure 5: Phase trajectory of the pressure signals registered by gauge p_{s-imp1} and its projections

showed the scale of growth of fluctuation of both derivatives which was much higher than in previous cases. This confirmed that the instability appeared much earlier in this location. According to numerous researchers [22] the onset of instabilities of blowers and low-head compressors can be expected in the inlet zone. At the transient phase, pressure p_{s-imp1} gradual decrement was continued whereas the derivatives kept constant rate of fluctuation. At the surge the system entered a large limit cycle enclosed between -2 kPa and 4 kPa.

The signal at p_{s-imp2} was registered at the blade mid-span (figure 6). Therefore it was expected that the phase trajectory plotted for this location was very similar to the previous one. Again, in this case high fluctuations of derivatives were observed in the inlet recirculation regime, i.e. at $t \in (6 \text{ s}, 9 \text{ s})$. Then the rate of fluctuations remained constant till the deep surge onset. At the deep surge, the pressure oscillated between -2 kPa and 4 kPa.

The phase portrait of dynamic signal at p_{s-imp3} is presented in figure 7. It can be observed that it showed no trace of the inlet recirculation. At $t \in (6 \text{ s}, 9 \text{ s})$ the rate of fluctuation of the derivatives remained unchanged. The phase portrait had the form of an ellipsoid moving along p_{s-imp3} axis. At the transient phase the rate of fluctuation of derivatives was increasing and then slightly decreased just before entering the deep surge. At deep surge the system entered a large limit cycle enclosed between 1 kPa and 8 kPa.

In all presented cases amplitude of fluctuation of both derivatives depended on the regime in which the blower operated. All projections $\overline{\overline{p_x}} - \overline{p_x}$ confirmed this statement. Phase portrait at $t < 6$ s had a form of an ellipse around $(0,0)$. As the system left the stable working conditions, ellipse radii corresponding to directions $\overline{p_x}$ and $\overline{\overline{p_x}}$ increased. At deep surge the oscillations had a more complex structure. Nevertheless, the distance from the point $(0,0)$ in both directions did not decrease. This observation allowed us to define the RDF parameter (section 3.2), that may play an important role in the early surge detection.
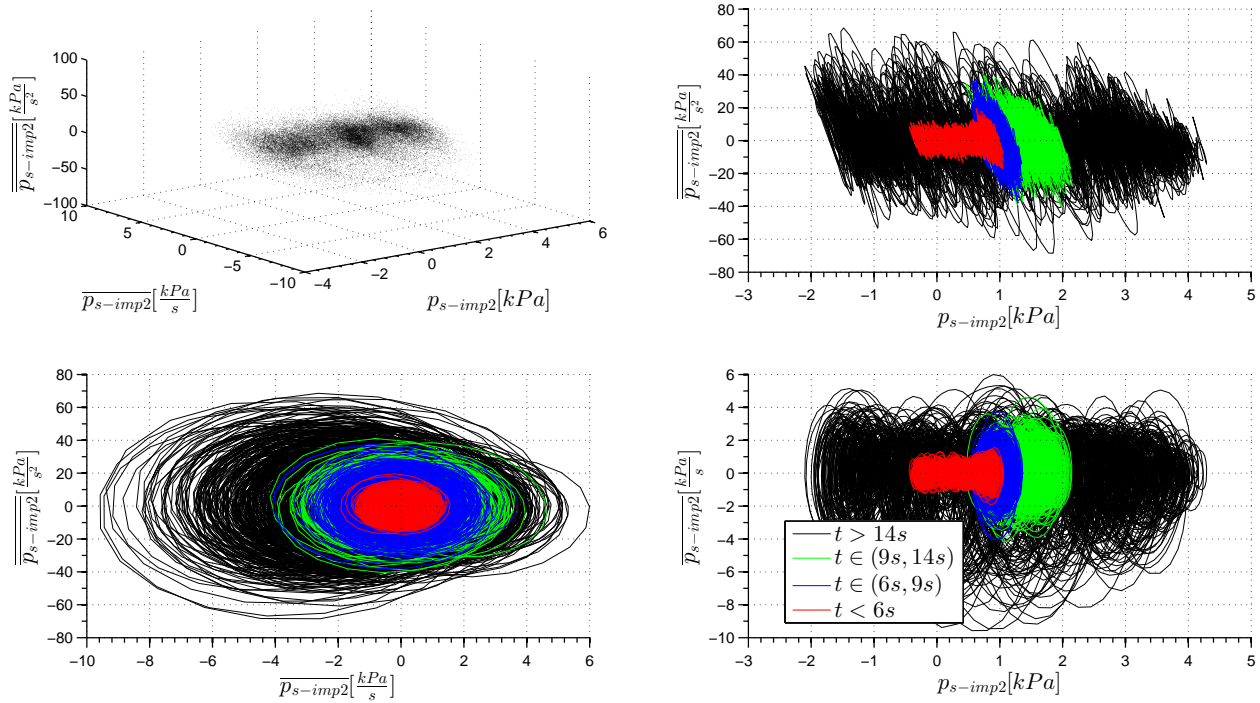
Figure 6: Phase trajectory of the pressure signals registered by gauge p_{s-imp2} and its projections

3.2 RDF Factor

Basing on findings presented in section 3.1 it was concluded that the instability can be measured by the following factor:

$$RDF = \frac{1}{\sqrt{2}} \sqrt{\frac{\left(\frac{dp}{dt}\right)^2}{\left(\frac{dp}{dt}\right)_D^2} + \frac{\left(\frac{d^2p}{dt^2}\right)^2}{\left(\frac{d^2p}{dt^2}\right)_D^2}} \quad (1)$$

This factor is referred to as the **Rate of Derrivative Fluctuation**, or shorter RDF. The main advantage of the RDF lies in the fact, that this parameter can be calculated at given moment of time based on the smoothed signal. Hence, it can be used for real-time monitoring. $(\cdot)_D$ in equation 1 indicates a value obtained individually for a particular machine. The normalization constant $\frac{1}{\sqrt{2}}$ came from the fact, that each of the elements of the sum was normalized to one and in the nominal working conditions the RDF attained the value of $\sqrt{1+1}$.

Figure 8 presents the values of RDF obtained at analysed pressure tappings. At the stable working conditions the RDF slightly oscillated around 1 at all gauges. Every permanent increment indicated that the rate of fluctuation of derivatives increased and the unstable structures appeared. Therefore, it was possible to define the threshold value RDF_t above which the anti-surge system could be activated. Too small value of the threshold may cause some false alarms, while too high would cause a delay in detection of dangerous unstable working conditions. Values around $RDF_t = 3$ seemed to be a reasonable compromise. RDF at the gauge p_{s-imp1} allowed to detect the inlet recirculation as early as in 7th second of the recorded signal. At p_{s-out} and p_{s-in} the value of 3 was reached around 9th and 10th second respectively. Both corresponded to the transient phase. Gauges p_{s-imp1} and
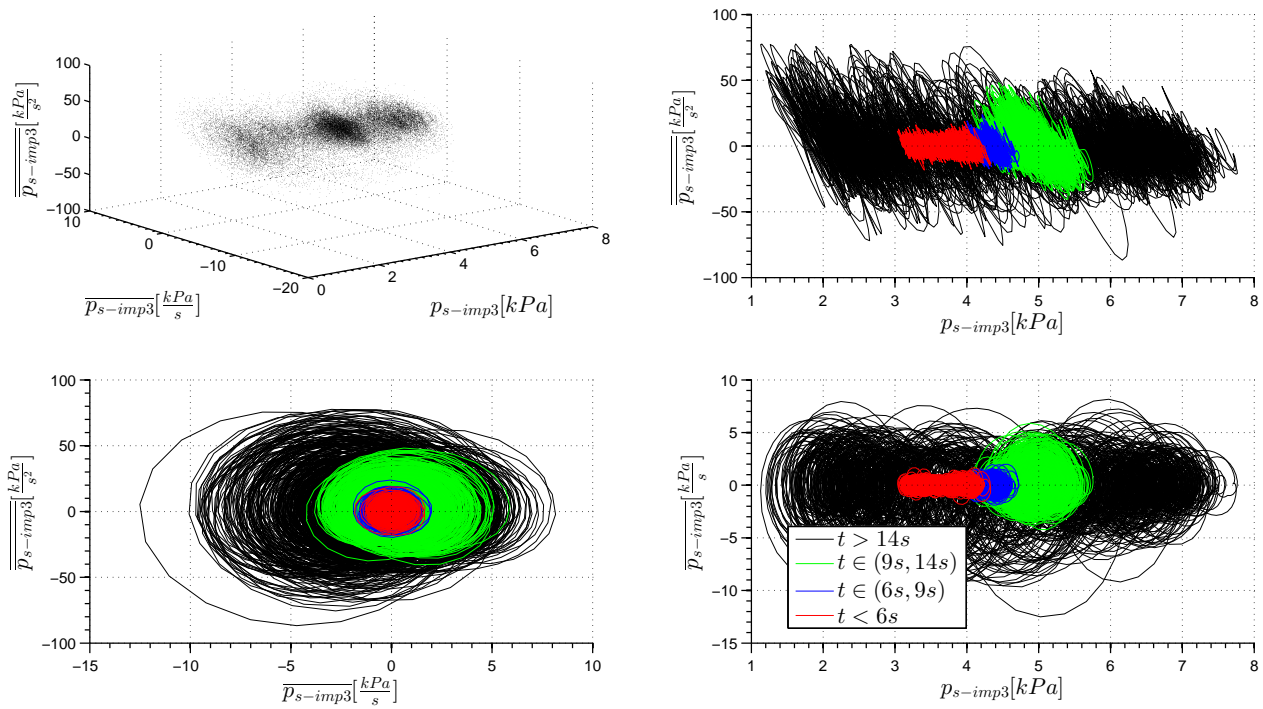
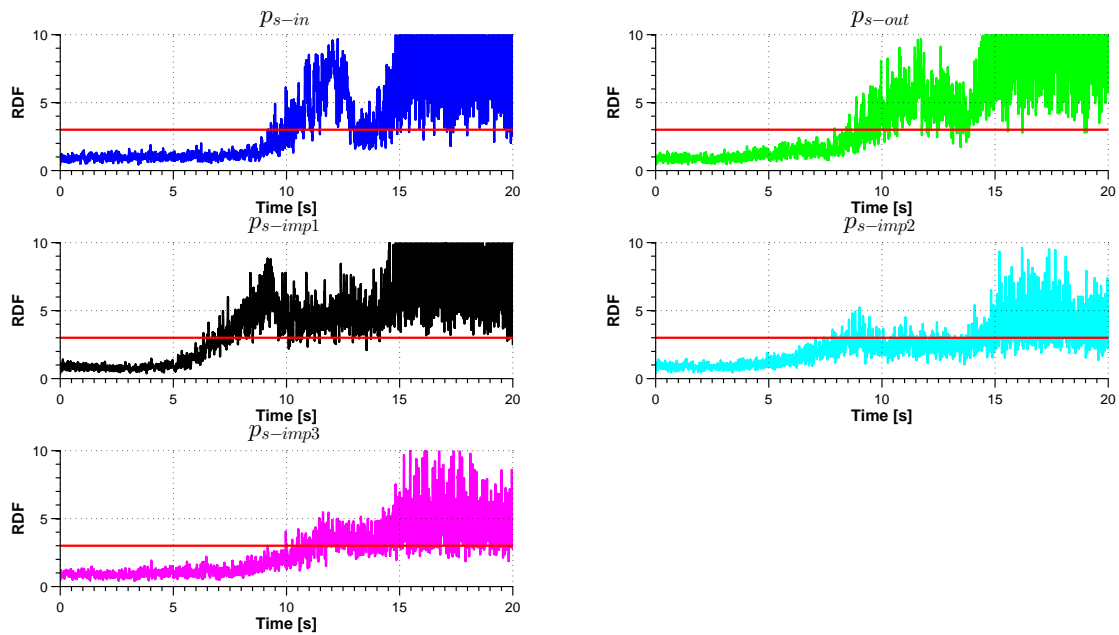Figure 7: Phase trajectory of the pressure signals registered by gauge p_{s-imp3} and its projections

Figure 8: RDF factor obtained at pressure tappings in dynamic tests and suggested threshold value ($RDF_t = 3$)

p_{s-imp2} are not recommended for detection of instabilities due to the risk of unintentional warning that may be caused by pressure fluctuations caused by the flow over blade tips.

The RDF can be monitored by a real-time controller. A Schematic block diagram of such a controller is presented in figure 9, where source signal is smoothed in order to reduce the noise. Then it is split into two branches and goes through single/double differentiating block. Afterwards, in each branch the signal is squared and multiplied by the normalization factor obtained at the design conditions. Next, signal is summed, goes through the square root block and $\frac{1}{\sqrt{2}}$ gain. At this point smoothing using a low pass filter can be added. Finally, as a result of this simple signal transformation, the RDF is obtained. If it exceeds the threshold value, the anti-surge system can be activated.
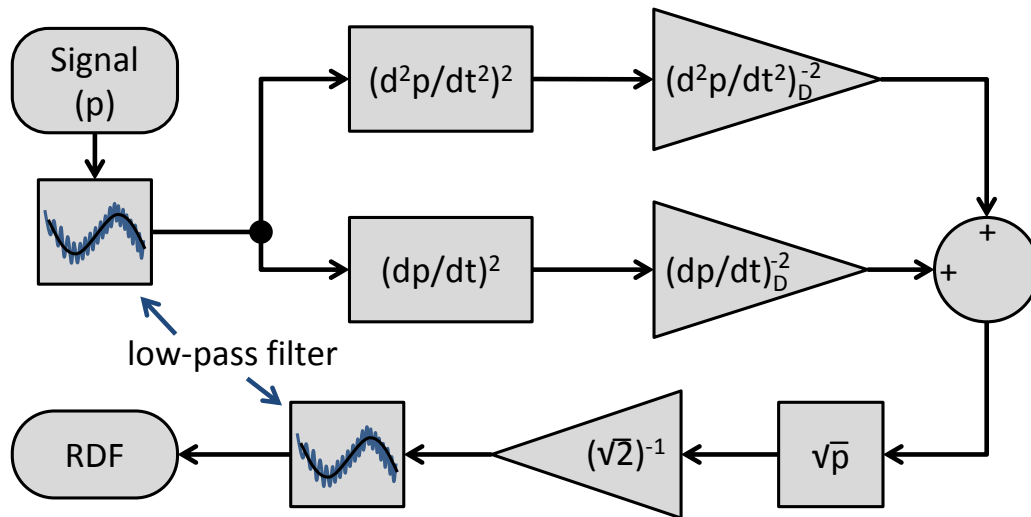

Figure 9: Block diagram of the controller for a real-time RDF measurement

4 DISCUSSION

The paper presents phase portraits of the pressure signals measured in different locations of the low speed centrifugal compressor. Based on the observations the RDF factor was proposed as a simple algorithm that could be used for an early indication of the danger of approaching surge. At stable working conditions the parameters keep values close to 1. When instability occurs in the system the RDF value starts to increase. When it exceeds the threshold value of 3 an anti surge system should be implemented.

Our solution provides very efficient surge protection that:

- allows compressors to be operated reliably close to the onset of surge which is of great importance for aerospace applications. This is big advantage over simple use of the anti-surge margin;

- is much cheaper than more advanced and active anti-surge systems;

- could be also used to monitor compressor working conditions and evaluate how close to optimal they are.

Technology is being developed. A new testing facility was built to make test runs of the anti-surge algorithms based on the presented concept. We are open to partnerships with institutions interested in testing this algorithm on their units and designs.

5   ACKNOWLEDGMENTS

6   REFERENCES

[1] Frigne, P. and den Braembussche, R.V., "Distinction Between Different Types of Impeller and Diffuser Rotating Stall in a Centrifugal Compressor With Vaneless Diffuser," *Journal of Engineering for Gas Turbines and Power*, Vol. 106, No. 2, 1984, pp. 468–474.

[2] Izmaylov, R., "Unsteady flow phenomena in centrifugal compressor: rotating stall and beyond," *Proceedings of 12th International Symposium on Unsteady Aerodynamics*, Imperial College, London, 2009.

[3] Greitzer, E., "The Stability of Pumping Systems—The 1980 Freeman Scholar Lecture," *Journal of Fluids Engineering*, Vol. 103, No. 2, 1981, pp. 193–242.

[4] van Helvoirt, J., *Centrifugal compressor surge: Modeling and identification for control*, Ph.D. thesis, University Microfilms International, P. O. Box 1764, Ann Arbor, MI, 48106, USA, 2007.

[5] de Jager, B., "Rotating stall and surge control: A survey," *Proceedings of the 34th Conference on Decision and Control*, IEEE, 1995.

[6] Stein, A., *Computational analysis of stall and separation control in centrifugal compressors*, Ph.D. thesis, Georgia Institute of Technology, 2000.

[7] Emmons, H., Pearson, C., and Grant, H., "Compressor surge and stall propagation," *Transactions of ASME*, Vol. 77, No. 4, 1955, pp. 455–467.

[8] Greitzer, E., "Surge and Rotating Stall in Axial Flow Compressors—Part I: Theoretical Compression System Model," *Journal of Engineering for Power*, Vol. 98, No. 2, 1976, pp. 190–198.

[9] Greitzer, E., "Surge and Rotating Stall in Axial Flow Compressors—Part II: Experimental Results and Comparison With Theory," *Journal of Engineering for Power*, Vol. 98, No. 2, 1976, pp. 199–211.

[10] Hansen, K., Jorgensen, P., and Larsen, P., "Experimental and theoretical study of surge in a small centrifugal compressor," *Journal of Fluids Engineering*, Vol. 103, No. 3, 1981, pp. 391–395.

[11] Willems, F., *Modeling and Bounded Feedback Stabilization of Centrifugal Compressor Surge*, Technische Universiteit Eindhoven, 2000.

[12] Meuleman, C., *Measurement and unsteady flow modelling of centrifugal compressor surge*, Ph.D. thesis, 2002.

[13] Chen, J., "Numerical simulation of stall and stall control in axial and radial compressors," Tech. rep., Mississippi State University, 2006.

[14] Bulot, N., Ottavy, X., and Trebinjac, I., "Unsteady pressure measurements in a high-speed centrifugal compressor," *Journal of Thermal Science*, Vol. 19, No. 1, 2010, pp. 34–41.

[15] Tamaki, H., "Experimental Study on Surge Inception in a Centrifugal Compressor," *International Journal of Fluid Machinery and Systems*, Vol. 2, No. 4, 2009, pp. 409–417.

[16] Lawless, P. and Fleeter, S., "Rotating Stall Acoustic Signature in a Low-Speed Centrifugal Compressor: Part 1—Vaneless Diffuser," *Journal of Turbomachinery*, Vol. 117, No. 1, 1995, pp. 87–96.

[17] Moore, F. and Greitzer, E., "A theory of post-stall transients in axial compression systems: Part I—Development of equations," *Journal of Engineering for Gas Turbines and Power*, Vol. 108, No. 1, 1986, pp. 68–76.

[18] Horodko, L., "Identification of rotating pressure waves in a centrifugal compressor diffuser by means of the wavelet cross-correlation," *International Journal of Wavelets, Multiresolution and Information Processing*, Vol. 4, No. 02, 2006, pp. 373–382.

[19] Turunen-Saaresti, T. and Larjola, J., "Unsteady pressure field in a vaneless diffuser of a centrifugal compressor: An experimental and computational analysis," *Journal of Thermal Science*, Vol. 13, No. 4, 2004, pp. 302–309.

[20] Horodko, L. and Kryłowicz, W., "Investigation of the Rotating Stall in a Centrifugal Compressor," *ASME Joint US-European Fluids Engineering Conference*, 2002.

[21] Horodko, L., "Investigation of Centrifugal Compressor Surge with Wavelet Methods," *Proceedings of 6-th European Conference on Turbomachinery, Fluid Dynamics and Thermodynamics*, VKI, Lile, 2005.

[22] Mizuki, S. and Oosawa, Y., "Unsteady flow within centrifugal compressor channels under rotating stall and surge," *Journal of Turbomachinery*, Vol. 114, No. 2, 1992, pp. 312–320.

[23] Kuz'min, V. and Khazhuev, V., "Measurement of liquid or gas flow (flow velocity) using convergent channels with a witoszynski profile," *Measurement Techniques*, Vol. 36, No. 3, 1993, pp. 288–296.